PHYSICAL-MECHANICAL PROPERTIES OF HIGH ENTROPY ALLOY $CrMnFeCoNi_2Cu$ IN TWO STRUCTURAL STATES IN THE TEMPERATURE RANGE OF 4.2–350 K

O. D. Tabachnikova[1], Yu. O. Shapovalov[1], S. M. Smirnov[2], V. F. Gorban[2], M. O. Krapivka[2], and S. O. Firstov[2]

[1]B.Verkin Institute for Low Temperature Physics and Engineering of NAS of Ukraine,47 Nauky Ave., Kharkiv, 61103, Ukraine

[2]I.M. Frantsevich Institute for Problems of Materials Sciences of the NASciences of Ukraine, 3 O. Pritsaka street, Kiev, 03142, Ukraine

E-mail: tabachnikova@ilt.kharkov.ua

In this work the mechanical properties of a high-entropy $CrMnFeCoNi_2Cu$ alloy with an fcc lattice have been studied in a broad temperature range 4.2–350 K in two structural states: the initial (state I) and after rolling up to 60% (state II).

Subject - high-entropy $CrMnFeCoNi_2Cu$ alloy with an fcc lattice.

Research methods - Structural studies of the obtained ingots were carried out by X-ray phase analysis, in the local Auger electron spectroscopy, and in the electron probe X-ray microanalysis. Hardness H and contact elastic modulus E were measured in accordance with the international standard ISO 14577-1:2002 (E). The mechanical tests were carried in the temperature range 4.2 – 300 K, with a relative deformation rate of 4×10^{-4} s^{-1} for compression strain and 10^{-4} s^{-1} for tensile deformation. During compression strain to $\varepsilon \approx 2\%$, the shear strain rate sensitivity $\Delta\tau/\Delta\ln \dot{\varepsilon}_a$ was determined as the $\dot{\varepsilon}_a$ strain rate increased from 4×10^{-4} s^{-1} to 1.8×10^{-3} s^{-1} (a factor of 4.4).

Alloy microstructure of the in different structural states

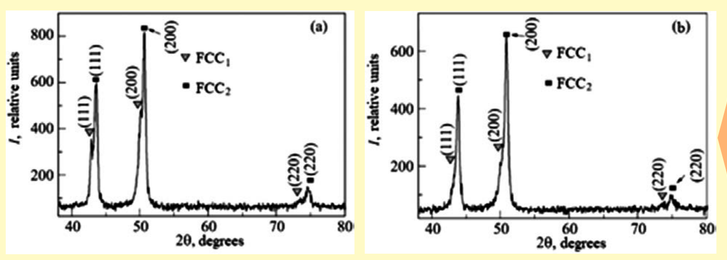

X-ray diffraction patterns of the high-entropy $CrMnFeCoNi_2Cu$ alloy structure in states I (a) and II (b). In both states I and II, two phases fcc are observed, i.e. rolling does not lead to additional phase transformations.

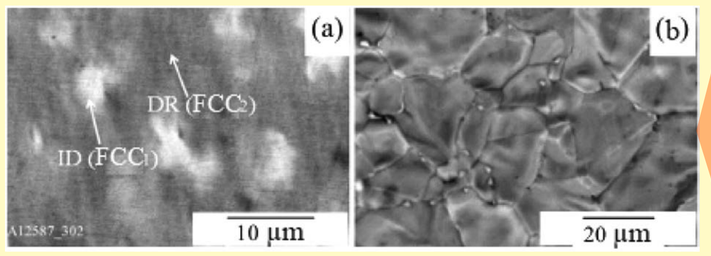

Typical images of the microstructure $CrMnFeCoNi_2Cu$ alloy in states I (a) and II (b).

The microstructure of the alloy in state I (a) contains light regions ranging in size from 5 to 10 μm against a dark background, which is consistent with the X-ray diffraction analysis results indicating a two-phase composition of the alloy. These light regions are enriched in copper and correspond to the fcc_1 phase, which has a larger lattice parameter than the fcc_2 phase (dark regions in (a)). Copper-rich areas are located in the interdendritic regions. In state II, the average grain size is ≈ 6 μm (b).

Numerical characteristics of the microstructure: M is the amount of the phase in weight percent, a is the lattice parameter, τ_i* is the texture coefficient, and i is the texture axis.

State of the sample	fcc_1			fcc_2		
	M, weight %	a, nm	τ_i* M, weight %	a, nm	τ_i*
I, initial	36.5	0.3633±4	$(0.50)_{200}$	63.5	0.3597±4	$(0.58)_{200}$
II, after rolling to 60%	12.6	0.3635±4	$(0.39)_{200}$	87.4	0.3589±4	$(0.34)_{200}$

Mechanical characteristics of the alloy $CrMnFeCoNi_2Cu$ in structural state II.

Hardness H and contact elastic modulus E of the $CrMnFeCoNi_2Cu$ alloy in structural states I and II.

Characteristics	State I	State II
H, GPa	2.6 ± 0.10	4.5 ± 0.11
E, GPa	122 ± 3	155 ± 5

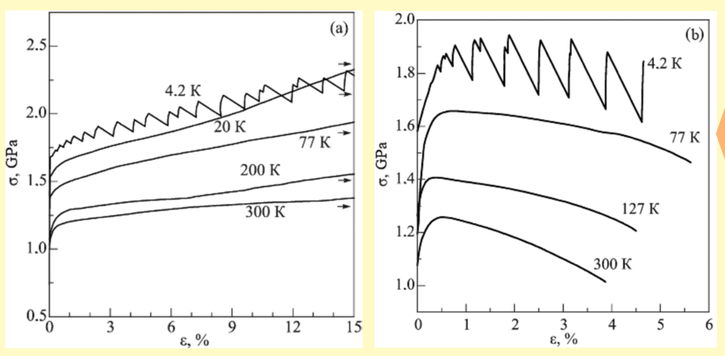

Typical stress–strain curves under compression (a) and tension (b) for various temperatures.

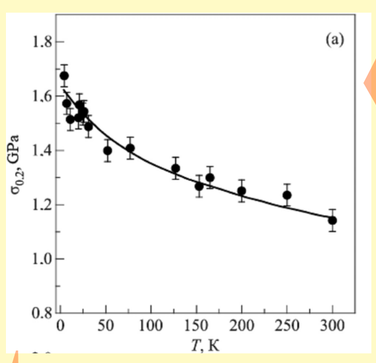

Temperature dependence tensile yield stress $\sigma_{0.2}$ under compression strain. The value of $\sigma_{0.2}$ increases monotonically from 1.14 to 1.68 GPa (by 47%) as the temperature decreases from 300 to 4.2 K (under tension, $\sigma_{0.2}$ increases from 1.11 to 1.70 GPa (by 53%)).

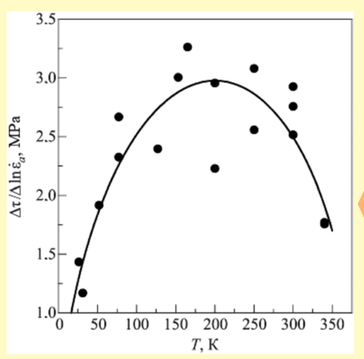

Temperature dependence of the shear strain rate sensitivity $\Delta\tau/\Delta\ln \dot{\varepsilon}_a$ at $\varepsilon \approx 2\%$. The solid line shows the theoretical dependence obtained using Eq. (8).

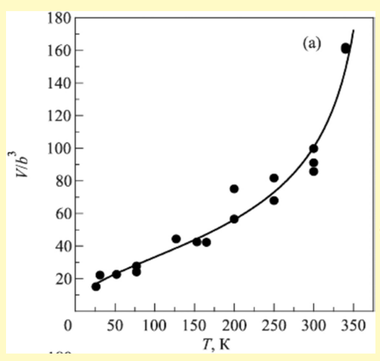

$$V(T) = kT\frac{\Delta \ln \dot{\varepsilon}_a}{\Delta \tau(T)} \quad (1)$$

Temperature dependence of the activation volume V/b3 at $\varepsilon \approx 2\%$ (b = 2.54×10^{-10} m. The solid line shows the theoretical dependence obtained using Eq. (6).

Thermal activation analysis of the mechanisms that control the plasticity of the studied alloy in state II

The theoretical formulas for the plastic strain rate $\dot{\varepsilon}$, effective stress τ^*, effective activation energy (enthalpy) $H(\tau^*)$, deforming stress $\tau(T)$, effective strain rate sensitivity, plastic strain activation volume V(T):

$$\dot{\varepsilon} = \dot{\varepsilon}_0 \exp\left[-\frac{H(\tau^*)}{kT}\right], \quad (2)$$

$$H(\tau^*) = H_0\left[1-\left(\frac{\tau^*}{\tau_c}\right)^p\right]^q, \quad (3)$$

$0 \le p \le 1, \quad 1 \le q \le 2$

$\tau^* = \tau - \tau_i$ – effective stress,

τ_i – internal stress

$$\tau(T) = \tau_i + \tau_c\left[1-\left(\frac{T}{T_0}\right)^{1/q}\right]^{1/p}, \quad (4)$$

$$\left(\frac{\partial\tau^*}{\partial \ln \dot{\varepsilon}}\right)_T = \frac{\tau_c}{pqA}\left(\frac{T}{T_0}\right)^{1/q}\left[1-\left(\frac{T}{T_0}\right)^{1/q}\right]^{(1-p)/p}, \quad (5)$$

$$V(T) = -\left(\frac{\partial H}{\partial \tau^*}\right)_T = \frac{pqH_0}{\tau_c}\left(\frac{T}{T_0}\right)^{1-1/q}\left(1-\left(\frac{T}{T_0}\right)^{1/q}\right)^{(p-1)/p}, \quad (6)$$

$A = \ln(\dot{\varepsilon}_a/\dot{\varepsilon})$ $T_0 = H_0/kA$

Experimental dependences (at $\varepsilon \approx 2\%$) were compared with theoretical dependences (4) and (5).

$$\tau_2(T) = \tau_i + \tau_c\left[1-\left(\frac{T}{T_0}\right)^{1/q}\right]^{1/P} \quad (7)$$

$$\left(\frac{\Delta\tau}{\Delta \ln \dot{\varepsilon}_a}\right)_T = \frac{\tau_c}{pqA}\left(\frac{T}{T_0}\right)^{1/q}\left[1-\left(\frac{T}{T_0}\right)^{1/q}\right]^{(1-P)/P} \quad (8)$$

$$A = -T\left(\frac{\Delta\tau}{\Delta \ln \dot{\varepsilon}_a}\right)_T^{-1} = \frac{d\tau_2}{dT}$$

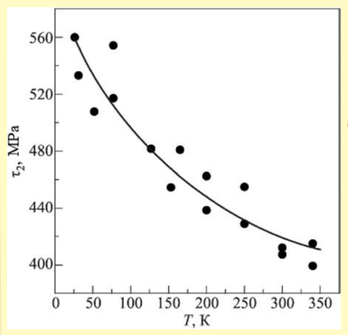

Temperature dependence of deforming stress τ_2 ($\varepsilon \approx 2\%$), state II. The solid line shows the theoretical dependence obtained using Eq. (7).

The theoretical values alloy parameters, obtained by analyzing of experimental data.

p	q	τ_i, MPa	τ_c, MPa	H_0, eV	T_0, K	A
2/3	1.6	408	206	0.82	382	25

Features of low temperature fracturing

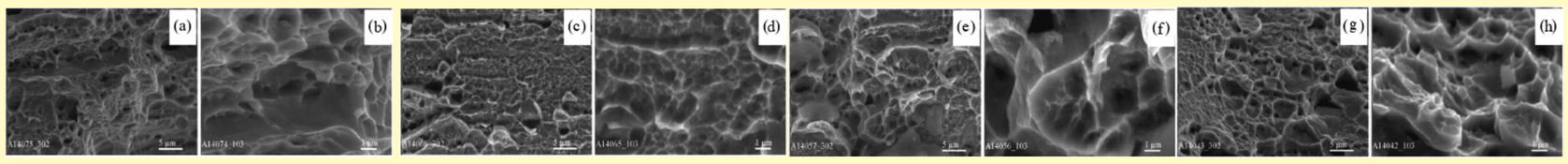

Fracture patterns observed on the fracture surface of samples in state II, after tensile deformation at various temperatures: 300 K (a), (b); 77 K (c),(d); 10 K (d), (e); and 4.2 K (g), (h). A typical ductile fracture is observed in the entire temperature range of 4.2–300 K.

Summary and conclusions

1. The microstructure and physical-mechanical properties of the high-entropy alloy $CrMnFeCoNi_2Cu$ were studied in two structural states: the initial state (state I) and after rolling up to 60% (state II).
2. It was found that in both states, the alloy contains two fcc phases differing in copper content. After rolling, the amount of the copper-rich phase decreases from 36.5 to 12.6 wt%.
3. When transitioning from state I to state II, microhardness increases from 2.6 to 4.5 GPa, and Young's modulus increases from 122 to 155 GPa.
4. In the temperature range of 4.2 – 300 K for state II, the patterns of plastic deformation and features of destruction under uniaxial tension and compression of samples were studied.
5. Temperature dependences of the yield strength σ0.2 were obtained, and the stages of the deformation curves were determined. It was established that, throughout the studied temperature range, the alloy exhibits a high-strength state while maintaining significant ductility. At all temperatures, the ductility of samples in state II under compression exceeds 15%, while under tension it is approximately 5%.
6. With a decrease in temperature from 300 K to 4.2 K, the value of $\sigma_{0.2}$ increases monotonically under compression deformation from 1.14 to 1.68 GPa (by 47%), and under tension from 1.11 to 1.7 GPa (by 53%).
7. At temperatures below ≈ 15 K, plastic deformation exhibits unstable behavior, manifested as jumps in strain stress on the stress-strain curves. These jumps occur immediately after reaching the yield point and continue until specimen failure. The average magnitude of the jumps in compression increases with strain, whereas in tension, it changes little at strains ≥ 1–2%. Jump-like plastic deformation is associated with slip localization and is determined by the combined action of interrelated dislocation-dynamic and thermal processes.
8. At all temperatures studied, the destruction remains viscous.
9. Based on experimental measurements of the temperature and strain rate dependences of the deforming stress (at ≈ 2% plastic strain) in the temperature range of 25 – 340 K, a thermal activation analysis of the processes controlling the deformation behavior of the alloy was performed. Empirical estimates of the microscopic parameters of plasticity, internal and effective stresses were obtained. It was shown that a single dislocation mechanism governing the thermally activated plasticity of the high-entropy alloy operates within the studied temperature range.
10. It was established that the distribution of barriers on dislocations corresponds to Friedel statistics, characteristic of thermally activated dislocation motion through a network of randomly distributed local obstacles. It was shown that the most probable local barriers controlling the process of thermally activated dislocation motion are atomic-scale structural inhomogeneities (atomic clusters) with an activation energy of $H_0 \approx 0.82$ eV. These clusters consist of several identical atoms and are located several nanometers apart.